International Journal of Dynamics and Control (2021) 9:1092–1099
https://doi.org/10.1007/s40435-020-00738-4

Discrete-time attitude stabilization of reusable reentry vehicle by convex optimization

Magdi S. Mahmoud[1] · Muhammad Maaruf[1]

Received: 10 August 2020 / Revised: 10 November 2020 / Accepted: 25 November 2020 / Published online: 1 January 2021

Abstract

This article addresses the attitude stabilization control of reusable reentry vehicle subjected to parametric variations and environmental perturbations. The nonlinear kinematic model of the vehicle is discretized and bluethen linearized using the global feedback linearization. A discrete time linear quadratic regulator with proportional-integral gain and disturbance rejection (LQRPI + D) is proposed to stabilized the system. The control formulation is based on convex optimization feasibility problem in terms of the linear matrix inequality. As illustrated by numerical simulations, the proposed technique provides better results compared to some existing methods.

Keywords Convex optimization · LQR · LMI · Reentry vehicle

1 Introduction

Reusable reentry vehicles are capable of carrying out tasks by flexible maneuvering on orbit [1]. The reusable reentry vehicles can be launched repeatedly, and have a lot of advantages such as cost effectiveness, speed and so on [2–4]. Because of these advantages, the vehicles are of high importance in civil and military aspects. Nevertheless, during the reentry process, the vehicle exhibits complicated coupling effects, strong nonlinearities, uncertainties and external perturbations which bring challenges to the development of the vehicle's attitude control [5–7]. Furthermore, several stringent constraints, such as dynamic pressure, heat flux, and structured loads add more challenges to the control design [8–10].

Over the past years, various control methods have been suggested for the vehicle's flight control. Earlier flight control problems were based on the linearized model of the aerocrafts at a particular operating point. In [11–14], a LQR has been designed to stabilized the reentry vehicle. However, this method is unsuitable for the multivariable and highly nonlinear model of the vehicle. A more effective control can be achieved by linearizing the model at different operating regions based on gain-scheduling [15–18]. Although gain-scheduling approach can solve some vehicle control problems, robustness and global stability of the system can not be guaranteed, particularly in the event of sudden parametric variations. In order to improve the nonlinear performance of the gain scheduling method, a trajectory linearization control was proposed in [19–22] and dynamic inversion control method was utilized in [23–26]. Nonetheless, the downside of these approaches is poor robustness against parametric uncertainties and modeling errors if built poorly.

A good robust control performance of the reentry vehicle has been achieved using the robust backstepping method [27,28]. A command filtered backstepping control of a hypersonic vehicle with dynamic perturbations has been studied in [29]. A robust attitude control of reusable reentry vehicle has been realized using the sliding mode control [30]. A fractional order sliding mode controller optimized with pigeon-inspired optimization has been developed for attitude control of the reentry vehicle [31]. In [32], a chattering-free sliding mode control of the reentry vehicle has been presented. A high-order sliding mode control was proposed for an uncertain space vehicle in the reentry period [33]. In [34], a robust model predictive control of the reentry vehicle has been investigated.

When the space vehicle is subjected to time-varying disturbances, an adaptive backstepping controller was utilized in [35]. In [36], an adaptive super-twisting sliding mode control

✉ Magdi S. Mahmoud
msmahmoud@kfupm.edu.sa

[1] Systems Engineering Department, KFUPM, P.O. Box 5067, Dhahran 31261, Saudi Arabia

was proposed for the vehicle in the reentry period. In [37], an adaptive fast terminal sliding mode control with disturbance observer has been designed for the reentry vehicle. In [38], a sliding mode based disturbance observer was designed for attitude control of a reentry vehicle with constrained inputs.

It is worth noting that the aforementioned control techniques are in continuous time domain. Recently, the applications of computer controlled systems are increasing due to the emergence of cheap micro-controllers with very fast sampling rates [39]. Dynamic systems such as reusable reentry vehicle requires controllers with very fast sampling rates. Therefore, discrete time control of reusable reentry vehicle is an important area to explore. In [40], attitude control of reentry hypersonic vehicle was achieved using a discrete time backstepping technique. In [41], a discrete time sliding control of reusable space vehicle vehicle was studied.

Motivated by the aforesaid discussion, this paper investigates the attitude optimal control of the reusable reentry vehicle subjected to external disturbances and parametric variations. Contrary to [1,2,6–38], the nonlinear kinematic model of the vehicle is transformed into a discrete time form using the Euler method. Unlike [11–18] where the nonlinear kinematic model of the vehicle was linearized near a particular operating point, we linearized the model using global feedback linearization. During the reentry phase, exact linearization is not possible due to parametric variations, coupled dynamics and disturbances. We modelled these effects as constant disturbances and a robust LMI based LQRPI + D is designed to tackle the problem. Unlike the robust control methods [27–41], a convex optimization is formulated to compute the optimal controller gains. Comparing with the conventional LMI based LQR, the innovation points of this article are as follows:

1. We proposed a robust LQRPI + D based on LMI to stabilized the reentry vehicle. This controller combines the advantages of convex optimization, disturbance suppression and quick convergence.
2. The impact of the disturbances is penalized by including a new cost term to the cost function.
3. In addition, a cost term representing the integral of the deviation of the output from the equilibrium is added to the objective function to minimize the deviation of the output from the equilibrium.

This paper is arranged as follows: The kinematic model of the reentry vehicle is provided in Sect. 2. In Sect. 3, the LQRP, LRQP + D and LQRPI + D are designed. Numerical simulations and discussions are given in Sect. 4. The research is concluded in Sect. 5.

2 Mathematical modelling

The complete model of the reentry vehicle is shown in Fig. 1. The attitude kinematic model of the reentry vehicle consists of three degree of freedom translational kinematic subsystem and three degree of freedom rotational kinematic subsystem. The nonlinear model is obtained under the following assumptions [34,35]

1. The vehicle is unpowered rigid body.
2. Rotational effect of the earth is ignored.
3. Slow movement of the vehicle is neglected.

Then, the nonlinear dynamic model of the reentry vehicle can be described as [34,35]

$$\dot{\alpha} = \zeta_y - \zeta_x\, cos\alpha\, tan\beta - \zeta_z\, sin\alpha\, tan\beta + \frac{1}{m\pi}(Y + mg\, cos\delta\, cos\mu). \tag{1}$$

$$\dot{\beta} = \zeta_x\, sin\alpha - \zeta_z\, cos\alpha + \frac{1}{m\pi}(Y + mg\, cos\delta\, sin\mu). \tag{2}$$

$$\dot{\mu} = -\zeta_x\, cosa\, cos\beta - \zeta_z\, sin\alpha\, cos\beta + \zeta_y sin\beta - \Big[\frac{1}{m\pi}(tan\beta + tan\delta\, sin\mu) - \frac{g\, cos\delta\, cos\mu\, tan\beta}{\pi} + \frac{Y\, tan\delta\, cos\mu}{m\pi}\Big]. \tag{3}$$

$$\dot{\zeta}_x = \frac{J_{zz}u_x}{J_{xx}J_{zz} - J_{xz}^2} + \frac{J_{xz}u_z}{J_{xx}J_{zz} - J_{xz}^2} + \frac{(J_{xx} - J_{yy} + J_{zz})J_{xz}}{J_{xx}J_{zz} - J_{xz}^2}\zeta_x\zeta_y + \frac{(J_{yy} - J_{zz})J_{zz} - J_{xz}^2}{J_{xx}J_{zz} - J_{xz}^2}\zeta_y\zeta_z. \tag{4}$$

$$\dot{\zeta}_y = \frac{u_y}{J_{yy}} + \frac{J_{xz}u_z}{J_{yy}}(\zeta_z^2 - \zeta_x^2) + \frac{J_{zz} - J_{xx}}{J_{xx}J_{zz} - J_{xz}^2}\zeta_x\zeta_z. \tag{5}$$

$$\dot{\zeta}_z = \frac{J_{zz}u_x}{J_{xx}J_{zz} - J_{xz}^2} + \frac{J_{xz}u_z}{J_{xx}J_{zz} - J_{xz}^2}$$

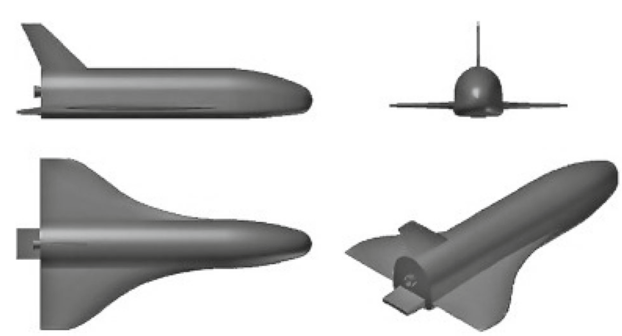

Fig. 1 The complete model of the vehicle [42]

$$+\frac{(J_{xx}-J_{yy})J_{xx}+J_{xz}^2}{J_{xx}J_{zz}-J_{xz}^2}\zeta_x\zeta_y + \frac{(J_{yy}-J_{xx}-J_{zz})J_{xz}}{J_{xx}J_{zz}-J_{xz}^2}\zeta_y\zeta_z. \quad (6)$$

where α, β, and μ stand for the attack angle, sideslip angle and bank angle respectively, g, L, m, π, Y, and δ denote the gravitational acceleration, aerodynamic lift force, side force, reentry velocity, flight path angle, and mass respectively; J_{xx}, J_{yy}, J_{zz}, & J_{xz} denote the moments of inertia. $u = [u_x\ u_y\ u_z]^T$ represent the control torque. The kinematic equations can be simplified as follows

$$\begin{cases} \dot{\Omega} &= f(\Omega) + g(\zeta)\zeta. \\ J\dot{\zeta} &= -\zeta^{\times} J\zeta + u. \end{cases} \quad (7)$$

where $\zeta = [\zeta_x\ \zeta_y\ \zeta_z]^T$ denote the angular velocity vector and $\Omega = [\alpha\ \beta\ \mu]^T$ is the attitude angle vector, $\zeta^{\times} \in \Re^{3\times3}$ is the skew-symmetric operator.

$$f(\Omega) = \begin{bmatrix} (-L + mg\ cos\delta\ cos\mu)/(mV\ cos\beta) \\ (Y + mg\ cos\delta\ sin\mu)/(m\pi) \\ (tan\beta\ + tan\delta\ sin\mu)L/(m\pi) - g\ cos\delta\ cos\mu\ tan\beta/\pi \\ +Y\ tan\delta\ cos\mu/(m\pi) \end{bmatrix}.$$

$$g(\Omega) = \begin{bmatrix} -cos\alpha\ tan\beta & 1 & -sin\alpha\ tan\beta \\ sin\alpha & 0 & -cos\alpha \\ -cos\alpha\ cos\beta\ sin\beta & & -sin\alpha\ cos\beta \end{bmatrix}.$$

$$J = \begin{bmatrix} J_{xx} & 0 & -J_{xz} \\ 0 & J_{yy} & 0 \\ -J_{xz} & 0 & J_{zz} \end{bmatrix} : \zeta^{\times} = \begin{bmatrix} 0 & -\zeta_z & \zeta_y \\ \zeta_z & 0 & -\zeta_x \\ -\zeta_y & \zeta_x & 0 \end{bmatrix}.$$

2.1 Discrete time model

The nonlinear model (7) can be transformed into a discrete-time model using the Euler method [42]. If the sampling interval is chosen as T_s, an approximate discrete time model can be derived as

$$\begin{cases} \Omega(k+1) = \Omega(k) + T_s f(\Omega(k)) + T_s g(\zeta(k))\zeta(k). \\ \zeta(k+1) = \zeta(k) - J^{-1}\zeta^{\times}(k)J\zeta(k) + T_s J^{-1}u(k). \end{cases} \quad (8)$$

2.2 Feedback linearization

Selecting the attitude angle vector, Ω, as the output, and u as the control input vector, the relative degree of the system (7) is (2,2,2). By using the approach presented in [43], the following equation can be obtained

$$\begin{aligned} \Omega(k+2) &= \Omega(k+1) + T_s f(\Omega(k+1)) \\ &\quad + T_s g(\zeta(k+1))\zeta(k+1). \\ &= \Omega(k+1) + T_s f(\Omega(k+1)) \\ &\quad + T_s g(\zeta(k+1))[\zeta(k) - J^{-1}\zeta^{\times}(k)J\zeta(k)] \\ &\quad + T_s^2 g(\zeta(k+1))J^{-1}u(k). \end{aligned} \quad (9)$$

Then, (9) can be rewritten as

$$\Omega(k+2) = F(\Omega(k), \zeta(k)) + G(\zeta(k))u(k). \quad (10)$$

where

$$\begin{aligned} F(\Omega(k), \zeta(k)) &= \Omega(k+1) + T_s f(\Omega(k+1)) \\ &\quad + T_s g(\zeta(k+1))[\zeta(k) - J^{-1}\zeta^{\times}(k)J\zeta(k)]. \\ G(\zeta(k)) &= T_s^2 g(\zeta(k+1))J^{-1}. \end{aligned}$$

From (10), the following discrete-time strict feedback system is derived

$$\begin{cases} \mathbf{X}_1(k+1) = \mathbf{X}_2(k). \\ \mathbf{X}_2(k+1) = F(\Omega(k), \zeta(k)) + G(\zeta(k))u(k). \end{cases} \quad (11)$$

where $\mathbf{X}_1(k) = \Omega(k)$, $\mathbf{X}_2(k) = \Omega(k+1)$. Equation (11) can be completely linearized using the following feedback control law

$$u(k) = G(\zeta(k))^{-1}[-F(\Omega(k), \zeta(k)) + v(k)]. \quad (12)$$

where $v(k) = [v_x\ v_y\ v_z]^T$ is the vector of the new inputs to stabilize the linearized system. Using (12), the exact linearized system is as follows

$$\begin{cases} \mathbf{X}_1(k+1) &= \mathbf{X}_2(k). \\ \mathbf{X}_2(k+1) &= v(k) + \Delta. \end{cases} \quad (13)$$

Remark 1 In real situation, exact feedback linearization is not possible due to the parametric uncertainties and external disturbances affecting the vehicle during the reentry phase. As such, Δ is added to (13) to account for the bounded disturbances.

Equation (13) can be rewritten as

$$\begin{cases} \mathbf{X}(k+1) = A_0\mathbf{X}(k) + B_0 v + \Gamma\Delta. \\ y(k) = C_0\mathbf{X}(k). \end{cases} \quad (14)$$

where $\mathbf{X}(k) = [\mathbf{X}_1(k)^T\ \mathbf{X}_2(k)^T]^T \in \Re^{1\times6}$, $A_0 \in \Re^{6\times6}$, $B_0 \in \Re^{6\times3}$, $\Gamma \in \Re^{6\times3}$ and $C_0 \in \Re^{3\times6}$ are given by

$$A_0 = \begin{bmatrix} 0 & I \\ 0 & 0 \end{bmatrix};\ B_0 = \begin{bmatrix} 0 \\ I \end{bmatrix};\ \Gamma = \begin{bmatrix} 0 \\ I \end{bmatrix};\ C_0 = \begin{bmatrix} I & 0 \end{bmatrix};$$
$$I = diag\{1, 1, 1\}.$$

Remark 2 Using Matlab, rank([B AB])=6 which is the same as the order of the system. Therefore, the linearized system is controllable.

3 Control design

In this section, LQRP, LQRP + D and LQRIP + D are formulated in terms LMI for the system (14). The block diagram of the closed loop system is shown in Fig. 2.

3.1 LQRP design

In this section, a LMI based LQRP is designed for (14) with $\Delta = 0$. Consider the following cost function

$$J = \sum_{k=0}^{\infty} [y_k^T Q y_k + v_k^T R v_k]. \tag{15}$$

where $Q > 0$ and $R > 0$ represent the output error and the control weighting matrices respectively. We go a head to establish the linear optimal control law $u(k) = L\mathbf{X}_k$ that stabilizes (14) while minimizing (15). Assuming that the Lyapunov function V_k has the following properties:

$$V_k = \mathbf{X}_k^T M \mathbf{X}_k, \quad M > 0. \tag{16}$$

There exists $\vartheta_+ > 0$ such that $\mathbf{X}_0^T M \mathbf{X}_0 \leq \vartheta_+$.

$$V_k \leq -[\mathbf{X}_k^T C^T Q C \mathbf{X}_k + v_k^T R v_k]. \tag{17}$$

Then, (14) under v_k is asymptotically stable and $J_\infty \leq V(\mathbf{X}_0)$. Using $v_k = L\mathbf{X}_k$, one has

$$\begin{aligned} &\mathbf{X}_k^T [M(A + BL) + (A + BL)^T M^T]\mathbf{X}_k \\ &\quad \leq -\mathbf{X}_k^T [C^T Q C + L^T R L]\mathbf{X}_k. \end{aligned} \tag{18}$$

If there exists L and M such that $\mathbf{X}_k \neq 0$, one gets

$$M(A + BL) + (A + BL)^T M^T + C^T Q C + L^T R L \leq 0. \tag{19}$$

The upper bound on the cost $\mathbf{X}_0^T M \mathbf{X}_0$ can be minimized for a given ϑ_+ as

$$\min_{\vartheta_+, K, L} \vartheta_+ \ \ subject\ to\ (19)$$

Equation (19) can be expressed as

$$\Upsilon = \begin{bmatrix} \psi & C^T Q & L^T R \\ * & -Q * 0 & \\ * & * & -R \end{bmatrix} \leq 0. \tag{20}$$

where $\psi = M(A + BL) + (A + BL)^T M^T$. Pre- and post-multiplying (20) by $diag\{Y, I, I\}$ and considering $Y = M^{-1}$ and $S = LY$, the convex optimization of (19) is expressed as

$$\begin{bmatrix} (AY + BS) + (AY + BS)^T & YQ & YL^T R \\ * & -Q & 0 \\ * & * & -R \end{bmatrix} \leq 0,$$
$$\begin{bmatrix} \vartheta_+ & \eta_0^T \\ * & Y \end{bmatrix} \geq 0. \tag{21}$$

The bound of the Lyapunov function is thus

$$\begin{bmatrix} \vartheta_+ & \mathbf{X}_0^T \\ * & M^{-1} \end{bmatrix} \geq 0 \Leftrightarrow \begin{bmatrix} \vartheta_+ & \eta_0^T \\ * & Y \end{bmatrix} \geq 0. \tag{22}$$

After attaining a feasible solution, one has $L = SY^{-1}$, $M = Y^{-1}$

3.2 LQRP + D

The LQRP designed in Sect. 3.1 does not consider the effects of external disturbances and unmodeled dynamics. In order

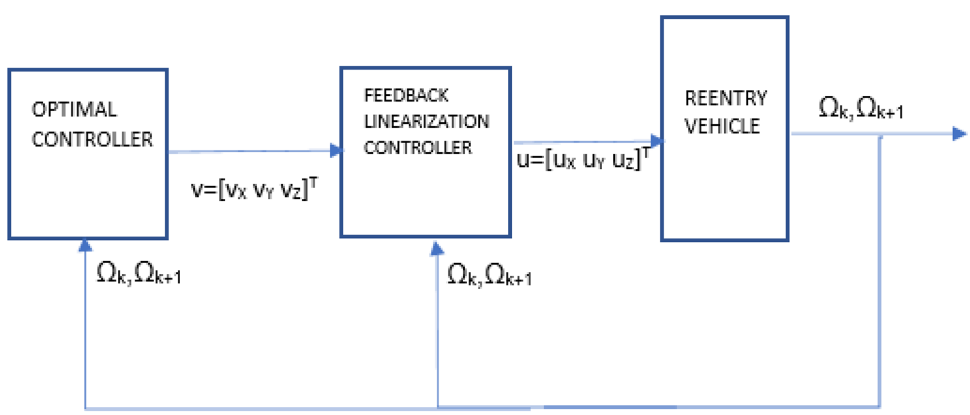

Fig. 2 The block diagram of the optimal control of the reentry vehicle

to account for these problems, a new cost term is added to the cost function (15). The modified cost function is given by

$$J = \sum_{k=0}^{\infty}[y_k^T \tilde{Q} y_k + \Omega v_k^T v_k - \Lambda^2 \Delta^T \Delta]. \tag{23}$$

Letting $\tilde{R} = diag[\Omega \quad -\Lambda^2]$ and $U_k = [v_k^T \quad \Delta^T]^T$, we get

$$J = \sum_{k=0}^{\infty}[y_k^T \tilde{Q} y_k + U_k^T \tilde{R} U_k]. \tag{24}$$

We define the following Lyapunov function to ensure closed loop stability

$$\tilde{V}_k = \mathbf{X}_k^T P \mathbf{X}_k, \quad \tilde{V}_k > 0. \tag{25}$$

There exists $\vartheta > 0$ such that $\mathbf{X}_0^T P \mathbf{X}_0 \leq \vartheta_+$. Then, it follows that

$$\tilde{V}_{k+1} \leq -[\mathbf{X}_k^T \tilde{Q} \mathbf{X}_k + U_k^T \tilde{R} U_k]. \tag{26}$$

Equation (14) under U_k is asymptotically stable and $J_\infty \leq \tilde{V}_k(\mathbf{X}_0)$. Substituting $U_k = H\mathbf{X}_k$ into (26) yields

$$\mathbf{X}_k^T[P(A+GH) + (A+GH)^T P^T]\mathbf{X}_k \leq -\mathbf{X}_k^T[\tilde{Q} + H^T \tilde{R} H]\mathbf{X}_k. \tag{27}$$

where $G = [B \quad \Gamma]$. If there exist H and P with $\mathbf{X}_k \neq 0$, (27) becomes

$$P(A+GH) + (A+GH)^T P^T + \tilde{Q} + H^T \tilde{R} H \leq 0. \tag{28}$$

The minimization problem can be written as

$$\min_{\vartheta_+, P, H} \vartheta_+ \ \textit{subject to}\ (28)$$

Using the same approach as the foregoing section, we have

$$\begin{bmatrix} (AZ+BT) + (AZ+BT)^T & ZC^T\tilde{Q} & ZF^T\tilde{R} \\ * & -\tilde{Q} & 0 \\ * & * & -\tilde{R} \end{bmatrix} \leq 0.$$

$$\begin{bmatrix} \vartheta_+ & \eta_0^T \\ * & Z \end{bmatrix} \geq 0. \tag{29}$$

On reaching feasible solution, one gets $H = TZ^{-1}$, $P = Z^{-1}$.

3.3 LQRPI + D

In this section, the LQRP + D formulation is modified by including an extra cost term denoting the integral of the deviation of the output from its initial state, $\theta = \int_0^t y(\tau)d\tau$ ($\dot{\theta} = Cx$). The discrete time equivalent of the integral of the output can be expressed as

$$\varepsilon_{k+1} = C\mathbf{X}_k. \tag{30}$$

where $\varepsilon_{k+1} = \theta_{k+1} - \theta_k$. The new cost function is given by

$$J = \sum_{k=0}^{\infty}[y_k^T y_k + \varepsilon_k^T \varepsilon_k + \sigma v_k^T v_k - \Lambda^2 \Delta^T \Delta]. \tag{31}$$

Introducing $U_k = [v_k^T \quad \Delta^T]^T$, $\chi = [\mathbf{X}_k^T \quad \varepsilon_k^T]^T$, we obtain

$$\begin{aligned} \dot{\chi} &= \begin{bmatrix} A & 0 \\ C & 0 \end{bmatrix}\chi + \begin{bmatrix} B \\ 0 \end{bmatrix} v_k + \begin{bmatrix} \Gamma \\ 0 \end{bmatrix}\Delta, \\ &= \hat{A}\chi + \hat{B}v_k + \hat{\Gamma}\Delta. \end{aligned} \tag{32}$$

Equation (31) can be rewritten as

$$J = \sum_{k=0}^{\infty}[\chi_k^T \hat{Q} \chi_k + U_k^T \hat{R} U_k]. \tag{33}$$

where

$$\hat{Q} = \begin{bmatrix} C^T C & 0 \\ 0 & \vartheta I \end{bmatrix}; \quad \hat{R} = \begin{bmatrix} \sigma I & 0 \\ 0 & \Lambda^2 I \end{bmatrix}.$$

We consider the following Lyapunov function

$$\hat{V}_k = \mathbf{X}_k^T \hat{P} \mathbf{X}_k, \quad \hat{V}_k > 0. \tag{34}$$

There exists $\vartheta > 0$ such that $\chi_0^T \hat{P} \chi_0 \leq \vartheta_+$. Then,

$$\hat{V}_{k+1} \leq -[\chi_k^T \hat{Q} \chi_k + U_k^T \hat{R} U_k]. \tag{35}$$

Using $U_k = \hat{H}\mathbf{X}_k$, $\forall \chi \neq 0$, we have

$$\hat{P}(\hat{A} + \hat{G}\hat{H}) + (\hat{A} + \hat{G}\hat{H})^T \hat{P}^T + \hat{Q} + \hat{H}^T \hat{R} \hat{H} \leq 0. \tag{36}$$

where $\hat{G} = [\hat{B} \quad \hat{\Gamma}]$. The minimization problem is thus

$$\min_{\vartheta_+, \hat{P}, \hat{H}} \vartheta_+ \ \textit{subject to}\ (36)$$

Based on convex analysis, problem (36) is converted to

$$\begin{bmatrix} (\hat{A}\hat{Z}+\hat{B}\hat{T})+(\hat{A}Z+\hat{B}\hat{T})^T & \hat{Z}C^T\hat{Q} & \hat{Z}\hat{F}^T\hat{R} \\ * & -\hat{Q} & 0 \\ * & * & -\hat{R} \end{bmatrix} \le 0.$$

$$\begin{bmatrix} \vartheta_+ & \eta_0^T \\ * & \hat{Z} \end{bmatrix} \ge 0. \tag{37}$$

A feasible solution gives $\hat{H}=\hat{T}\hat{Z}^{-1}$, $\hat{P}=\hat{Z}^{-1}$.

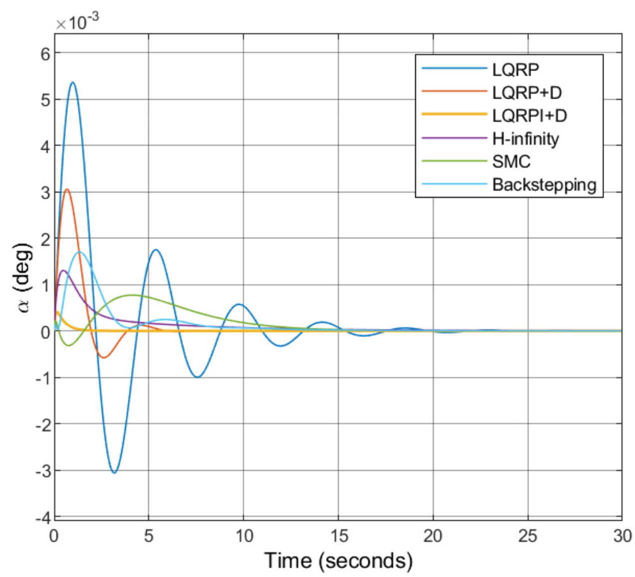

Fig. 3 Attack angle response

4 Simulation results

Numerical simulations are presented in this section to illustrate the efficacy of the proposed scheme. The simulations are carried out using the LMI MATLAB toolbox. Moreover, a comparison is made with an existing discrete time backstepping [40], discrete time sliding mode control [41] and LMI based H_∞ control [44]. The parameters of the reentry vehicle are adopted from [34]. The external disturbances and parametric uncertainties are modelled as constants $\Delta = [0.1\ 0.4\ 0.3]^T$. The weight matrices are chosen as $Q = C^T C$ and $R = 0.01$.

The simulation results are presented in Figs. 3, 4 and 5. The response of the angle of attack is depicted in Fig. 3. Due to the presence of the disturbances, the LQRP struggle to stabilized the attack angle. The LQRP + D, H_∞, sliding mode control and backstepping are able to suppress the disturbances and improve the performance of the LQRP. The LQRPI + D has the least overshoot and converge to zero at a quicker rate. In Fig. 4, the bank angle response is plotted. It can be seen that the LQRPI + D provides superior performance compared to the LQRP, LQRP + D, H_∞, sliding mode control and backstepping with respect to overshoot and settling time. The sideslip angle response is shown in Fig. 5. The sideslip angle is stabilized to zero at a faster rate under the action of LQRPI + D compared to the LQRP, LQRP + D, H_∞, sliding mode control and backstepping. The superior performance of the proposed LMI based LQRPI + D is due to its optimal gains, disturbance rejection capability and integral action.

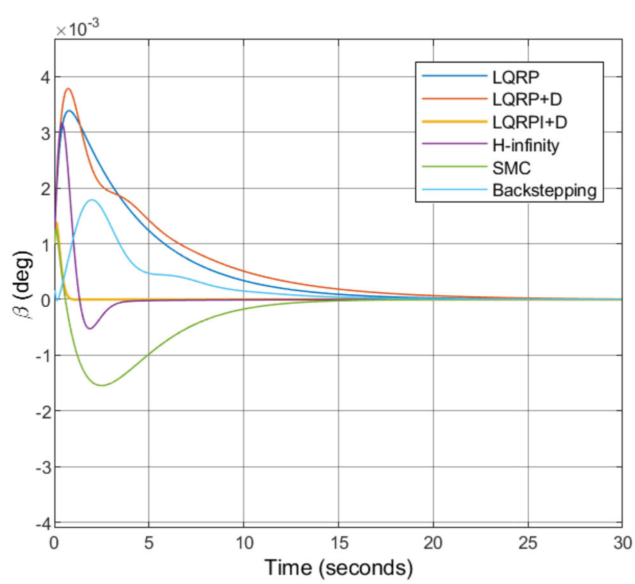

Fig. 4 Side slip angle response

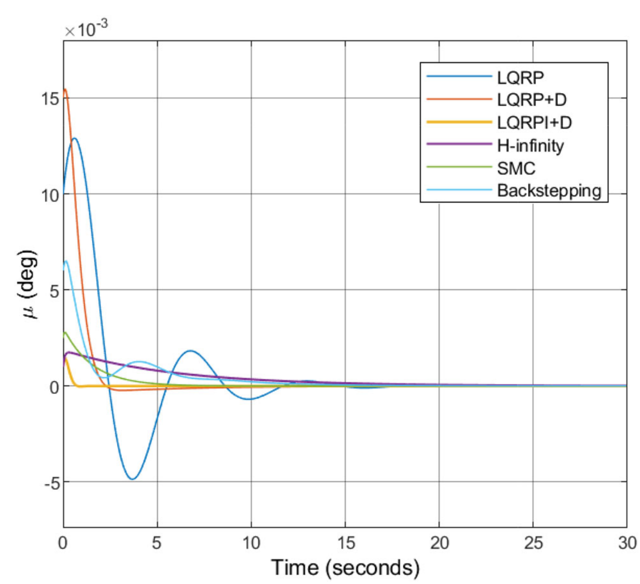

Fig. 5 Bank angle response

5 Conclusions

This paper presents LQRPI + D based on LMI optimization to stabilized the attitude angle of the reentry vehicle, by considering the external disturbances and parametric variations. The stability of the proposed controller is proved by Lyapunov function. Simulation results illustrate that the LQRPI + D can mitigate the effects of the external perturbations and enhance the vehicle robust control action. In addition, the proposed LQRPI + D outperforms LQRP, LQRP + D and H_∞.

Acknowledgements Funding was provided by King Fahd University of Petroleum and Minerals (Grant No. DUP 19106).

References

1. Li MM, Hu J (2018) An approach and landing guidance design for reusable launch vehicle based on adaptive predictor corrector technique. Aerosp Sci Technol 75:13–23
2. Wu X (2020) Grey wolf optimizer based active disturbance rejection controller for reusable launch vehicle. In: Proceedings of 2019 Chinese intelligent systems conference. CISC 2019. Lecture Notes in Electrical Engineering, vol 592. Springer, Singapore
3. Long L, Li P, Qin X, Mou Y (2018) The review on China space transportation system of past 60 years. Astronaut Syst Eng Technol 2(2):1–6
4. Sziroczak D, Smith H (2016) A review of design issues specific to hypersonic flight vehicles. Prog Aerosp Sci 84:1–28
5. Liu S, Liang Z, Ren Z, Li Q (2016) Review of reentry guidance methods for hypersonic gliding vehicles. Chin Space Sci Technol 36(6):1–13
6. Shaoming H, Tao S, Defu L (2017) Impact angle constrained integrated guidance and control for maneuvering target interception. J Guid Control Dyn 40(10):2653–2661
7. Viviani A, Iuspa L, Aprovitola A (2017) An optimization-based procedure for self-generation of re-entry vehicle shape. Aerosp Sci Technol 68:123–134
8. Fang Q, Li X (2008) Optimal trajectory planning and guidance research for hypersonic unpowered glider in near space. J Astronaut 29(5):1485–1491
9. Tian BL et al (2015) Real-time trajectory and attitude coordination control for reusable launch vehicle in reentry phase. IEEE Trans Ind Electron 62(3):1639–1649
10. Li Z et al (2019) Time-coordinated reentry guidance law for reusable launch vehicle. In: 2019 IEEE international conference on unmanned systems (ICUS), Beijing, China, pp 348–355
11. Hiroyuki I, Naohiko A, Makoto K (1986) Disturbance attenuation by a frequency-shaped linear-quadratic-regulator method. J Guid Control Dyn 9(4):397–402
12. Gauri PV, Kumar RH (2018) A comparison of optimal LQR controller and robust H_∞ controller for RLV. In: 2018 second international conference on intelligent computing and control systems (ICICCS), Madurai, India, pp 1055–1060
13. Dukeman G (2002) Profile-following entry guidance using linear quadratic regulator theory. 2002 AIAA guidance, navigation, and control conference and exhibit
14. Lu Q, Zhou J (2017) LQR tracking guidance law for hypersonic vehicle. In: 2017 29th Chinese control and decision conference (CCDC), Chongqing, pp 7090–7094
15. Kerr M, Marcos A, Pein L, Bornschlegl E (2008) Gain scheduled FDI for a re-entry vehicle. 2008 AIAA guidance, navigation and control conference and exhibit, p 7266
16. Al-sunni FM, Lewis FL (1992) Gain scheduling simplification by simultaneous control design. J Guid Control Dyn 16:602–603
17. Huang X et al (2013) Adaptive augmentation of gain-scheduled controller for aerospace vehicles. J Syst Eng Electron 24(2):272–280
18. Huang Y, Sun C, Qian C, Wang L (2013) Slow–fast loop gain-scheduled switching attitude tracking control for a near-space hypersonic vehicle. Proc Inst Mech Eng Part I J Syst Control Eng 227(1):96–109
19. Shao X, Wang H (2015) Active disturbance rejection based trajectory linearization control for hypersonic reentry vehicle with bounded uncertainties. ISA Trans 54:27–38
20. Su XL, Yu JQ, Wang YF, Wang LI (2013) Moving mass actuated reentry vehicle control based on trajectory linearization. Int J Aeronaut Space Sci 14(3):247–255
21. Xingling S, Honglun W (2014) Sliding mode based trajectory linearization control for hypersonic reentry vehicle via extended disturbance observer. ISA Trans 53(6):1771–1786
22. Zhang H, Yu Y, Wang H, Liu Y (2018) Reduced-order linear extended state observer based trajectory linearization control for hypersonic reentry vehicle under high maneuver flight with multiple disturbances. In: 2018 IEEE CSAA guidance, navigation and control conference (CGNCC), Xiamen, China, pp 1–6
23. Laxman R, Maity A, Mallikarjun RG, Kranthi KR (2020) Optimal nonlinear dynamic inversion-based flight control system design for an aerospace vehicle. In: Advances in small satellite technologies. Lecture notes in mechanical engineering. Springer, Singapore, pp 65–86
24. Acquatella BP, Briese LE, Schnepper K (2020) Guidance command generation and nonlinear dynamic inversion control for reusable launch vehicles. Acta Astronaut 174:334–346
25. Swaminathan S (2019) Robust lateral-directional flight control design for re-entry vehicles using dynamic inversion and sliding mode synthesis. In: 2019 fifth Indian control conference (ICC), New Delhi, India, pp 301–306
26. Sachin K, Shripad PM (2017) Design of thermal protection system for reusable hypersonic vehicle using inverse approach. J Spacecr Rock 54(2):436–446
27. Xingling S, Honglun W (2016) Back-stepping robust trajectory linearization control for hypersonic reentry vehicle via novel tracking differentiators. J Frankl Inst 353(9):1957–1984
28. Wang F et al (2019) Disturbance observer based robust backstepping control design of flexible air-breathing hypersonic vehicle. IET Control Theory Appl 13(4):572–583
29. Xiuyun Z et al (2020) Improved finite-time command filtered backstepping fault-tolerant control for flexible hypersonic vehicle. J Frankl Inst 357(13):8543–8565
30. Wang L, Liu Y, Liu X (2017) A novel global sliding mode control strategy for attitude control of reusable launch vehicles in the reentry phase. In: 2017 36th Chinese control conference (CCC), Dalian, pp 3615–3620
31. Xue Q, Duan H (2017) Robust attitude control for reusable launch vehicles based on fractional calculus and pigeon-inspired optimization. IEEE CAA J Autom Sin 4(1):89–97
32. Shen C et al (2016) An improved chattering-free sliding mode control with finite time convergence for reentry vehicle. In: IEEE Chinese guidance, navigation and control conference (CGNCC), Nanjing, pp 69–74
33. Bailing T et al (2013) Quasi-continuous high-order sliding mode controller design for reusable launch vehicles in reentry phase. Aerosp Sci Technol 28(1):198–207

34. Yang L et al (2017) Robust entry guidance using multi-segment linear pseudo spectral model predictive control. J Syst Eng Electron 28(1):103–125
35. Zhen W, Zhong W, Yijiang D (2016) Robust adaptive backstepping control for reentry reusable launch vehicles. Acta Astronaut 126:258–264
36. Yao Z, Shengjing T, Jie G (2017) Adaptive-gain fast super-twisting sliding mode fault tolerant control for a reusable launch vehicle in reentry phase. ISA Trans 71(2):380–390
37. An B, Wang B, Wang Y, Liu L (2019) Adaptive terminal sliding mode control for reentry vehicle based on nonlinear disturbance observer. IEEE Access 7:154502–154514
38. Fang W, Changchun H, Qun Z (2019) Novel smooth sliding mode attitude control design for constrained re-entry vehicle based on disturbance observer. Int J Syst Sci 50(1):75–90
39. Sowmiya C et al (2019) Further mean-square asymptotic stability of impulsive discrete-time stochastic BAM neural networks with Markovian jumping and multiple time-varying delays. J Frankl Inst 356(1):561–591
40. Zijun R, Wenxing F, Jie Y, Bin X (2017) Discrete reconfigurable back-stepping attitude control of reentry hypersonic flight vehicle. Adv Mech Eng 9(4):1–10
41. Swathy MV et al (2018) Discrete sliding mode control technique applied to reusable launch vehicle. In: 2018 international CET conference on control, communication, and computing (IC4), pp 1–4
42. Khan R, Raza A, Malik FM (2019) Sampled data control of nonlinear systems using extended order high gain observer. Int J Dyn Control 7:178–184
43. Cui R, Yang C, Li Y, Sharma S (2017) Adaptive neural network control of AUVs with control input nonlinearities using reinforcement learning. IEEE Trans Syst Man Cybern Syst 47(6):1019–1029
44. Mahmoudi M, Safari A (2019) LMI based robust control design for multi-input-single-output DC/DC converter. Int J Dyn Control 7:379–387